Wideband MIMO Directional Antenna Array with a Simple Meta-material Decoupling Structure for X-Band Applications

Jianfeng Jiang [1], Yingsong Li [1,2,*], Lei Zhao [3], and Xiaoguang Liu [4]

[1] College of Information and Communication Engineering
Harbin Engineering University, Harbin, 150001, China
[*]liyingsong@ieee.org

[2] Key Laboratory of Microwave Remote Sensing
Chinese Academy of Sciences, Beijing, 100190, China

[3] School of Information and Control Engineering
China University of Mining and Technology, Xuzhou, 221116, China

[4] Department of Electrical and Computer Engineering
University of California, Davis, 95618, China

Abstract ─ In this paper, a compact wideband MIMO directional antenna array with a single-layered meta-material is proposed to realize high isolation. The meta-material decoupling structure, which is composed of a modified split-rings and a square loop structure, is suspended over the two antenna elements to reduce the mutual coupling. The achieved results show that the proposed antenna array owns a −10 dB impedance bandwidth ranging from 8.5 GHz to 11.5 GHz. Furthermore, by loading the proposed meta-material superstrate over the two-element MIMO antenna, the designed MIMO antenna array not only has good performance but also enhances the isolation to be more -15 dB within the operating frequency band. In addition, the performances of the proposed antenna array are also tested by radiation pattern, gain, envelope correlation coefficient, diversity gain, total active reflection coefficient and so on. Therefore, these simulation results prove that the proposed wideband MIMO directional antenna array is a suitable candidate for X-band communication.

Index Terms ─ Directional, high isolation, low mutual coupling, low mutual coupling, meta-material, MIMO antenna, wideband, X-band.

I. INTRODUCTION

The X-band (8–12 GHz) of the radio spectrum is used in many applications including satellite communications, and radar [1-3]. To improve the link quality at X-band, it is often desirable to use directional antennas for their higher gain, narrower beam width, and better interference tolerance [4]. Meanwhile, wideband technologies have also received extensive attention for their ability to support higher data transmission and multi-channel connectivity [5]. When the channel bandwidth is large, however, multipath fading can degrade of channel capacity [6]. Multiple-input multiple-output (MIMO) technology has been proposed to overcome some of these problems. Because multiple data signals can be transmitted simultaneously, MIMO technology can enable high-capacity communications without increasing the bandwidth or signal-to-noise ratio (SNR) [7,8]. Thus, combining wideband technology with MIMO technology has become a research focus, and will play an important role in the future wireless communications [9–11].

In addition, owing to the increasing demand for miniaturization and portability of modern wireless communication devices and the increased number of antennas in MIMO systems, the antenna array structure is becoming more and more compact. However, the close proximity of antenna elements will cause strong mutual coupling between the antenna elements. Mutual coupling in an MIMO antenna array is mainly due to three factors: (1) surface wave, (2) coupling between the adjacent feeding lines, (3) coupling caused by space electromagnetic field [12, 13]. If the mutual coupling effect is not considered in the MIMO wireless communication system, it may cause antenna performance deterioration [14, 15]. Therefore, it is essential to give a solution to reduce the mutual coupling effect.

Several techniques have been proposed to mitigate mutual coupling in arrays. These techniques can be broadly categorized as the following:

Submitted On: January 30, 2020
Accepted On: April 20, 2020

(1) The neutralization line techniques: in this method, the two antenna elements are connected by a microstrip line, and the phase of current passing through this microstrip is opposite to the phase of equivalent current of the mutual coupling, thereby achieving the decoupling effect [16–18].

(2) The defected ground structure (DGS) techniques: in [19–21], the DGS is etched in the ground plane between microstrip patch antennas to change the distribution of effective substrate permittivity and the distributed inductance and capacitance of microstrip line to reduce mutual coupling.

(3) The parasitic element decoupling techniques: in [22–24], the researchers use the indirect coupled field generated by the parasitic element to cancel the direct coupling field to weaken the mutual coupling.

(4) The pattern and space diversity techniques: in [25–27], the antennas are placed in an orthogonal fashion to reduce the mutual coupling by taking advantage of the polarization orthogonality.

(5) The meta-material decoupling techniques: in [28–30], the electromagnetic band gap (EBG) structures are placed between two antenna elements to increase the isolation. In [32–33], meta-surface walls are inserted between the two antennas to reduce the mutual coupling.

A disadvantage of these methods is that they invariably occupy a large space between the two antenna elements, which is contrary to the trend of miniaturization.

Placing a meta-material superstrate above the antennas presents a viable solution to reduce the coupling between the two antenna elements while ensuring the miniaturization of antenna [34, 35]. As a two-dimensional periodic artificial structure, the meta-material is a structure in which plurality of slot cells or ideal conductor patches are distributed in a plane with a specific arrangement [36]. The meta-material superstrate has been used in many antenna applications, such as gain enhancement [37], radar cross section (RCS) reduction [38], radar radome [39], polarization converter [40], and microwave absorber [41]. Thus, various configurations such as patch, square loop, circular ring and slot shapes have been used to design the meta-material superstrate. However, most of the meta-materials are utilized in the field of narrowband antenna developments because the bandwidth of meta-material is limited [42]. Traditionally, the bandwidth of meta-material can be broadened by cascading multiple substrate layers [43, 44]. But this method increases the overall thickness, complexity and cost of fabrication.

In this paper, a meta-material based mutual coupling reduction structure is proposed and demonstrated. As a proof-of-concept example, a single-layered meta-material superstrate is suspended over a two-element patch antenna array working in the frequency of 8.5–11.5 GHz. We demonstrate that the proposed meta-material structure can enhance the isolation between the two patch elements, resulting in a low mutual coupling of less than -15 dB.

The organization of the rest of the paper is as follows: In Section II, the evolution process and the final optimized configuration of MIMO wideband directional antenna array and meta-material superstrate are proposed. Section III demonstrates the simulated results and analyzes the characteristics of optimized wideband MIMO directional antenna array. Finally, a conclusion is made in the last section.

II. DESIGN OF THE PROPOSED ANTENNA ARRAY

Figure 1 shows the proposed antenna array which is composed of two layers including the radiating patch antenna array and the meta-material superstrate.

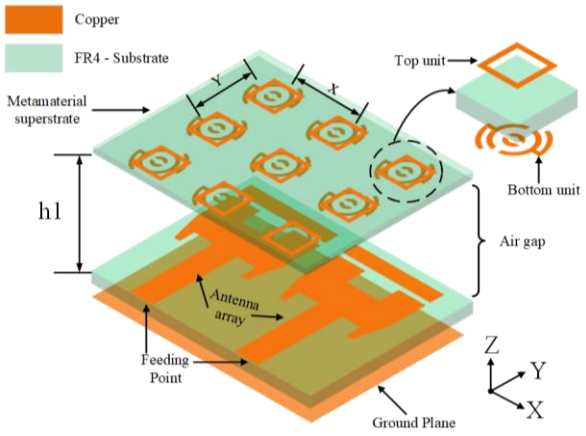

Fig. 1. Proposed MIMO antenna array with meta-material superstrate.

A. Design process of the antenna array

Microstrip patch antennas are widely used because of their low profile and ease of fabrication. However, a significant disadvantage of patch antennas is their narrow bandwidth. In order to improve the bandwidth, regular microstrip patch monopole antennas have been modified and optimized in this work. Figure 2 shows the evolution of the designs (denoted by antenna 1, 2, and 3, where antenna 3 is the final design used in this work). Figure 3 shows their respective S_{11}. The design starts from Antenna 1 with two identical monopole antennas, which have only two resonant frequency at 8 GHz and 13 GHz. In order to obtain a wider bandwidth, two rectangular parasitic patches are added as shown in Antenna 2. It can be seen that the higher resonant mode moved from 13 GHz to 12 GHz and impedance matching has been significantly improved over 10.5–12.5 GHz. However, the reflection coefficient of Antenna 2 over 8.5–10.5 GHz is still higher than −10

dB. Then, slot and beveled edge are added into the patch element to improve the impedance match over 8.5–10.5 GHz as shown as Antenna 3. Figure 3 shows that the lower resonant frequency shift to 9 GHz and the bandwidth range from 8.5 GHz to the 12.5 GHz.

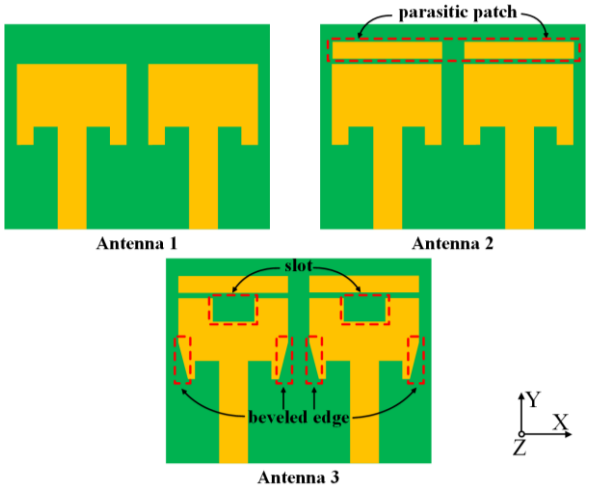

Fig. 2. Design process of the proposed wideband MIMO directional antenna array.

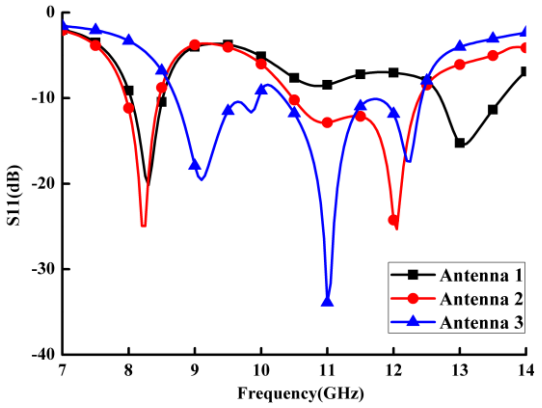

Fig. 3. The simulated S_{11} with evolution from antenna 1 to 3.

Figure 4 shows the top view and bottom view of the final design and the critical dimensions of the two-element patch antenna are presented in Table 1. The two-element antenna array is integrated on the top of a FR4 substrate with a thickness of 1.6 mm, a relative permittivity of 4.4 and a loss tangent of 0.02. The ground plate acts as a reflector covering almost the entire bottom surface. The proposed two-element radiating patch has an overall dimension of $30 \times 22 \times 1.6$ mm^3. Besides, as can be seen from the figure, the edge-to-edge distance between the two radiating antenna elements is only 2.3 mm (0.076 λ_0, where λ_0 refers to the wavelength of 10 GHz in vacuum), which is very compact and suitable for use in miniaturized devices.

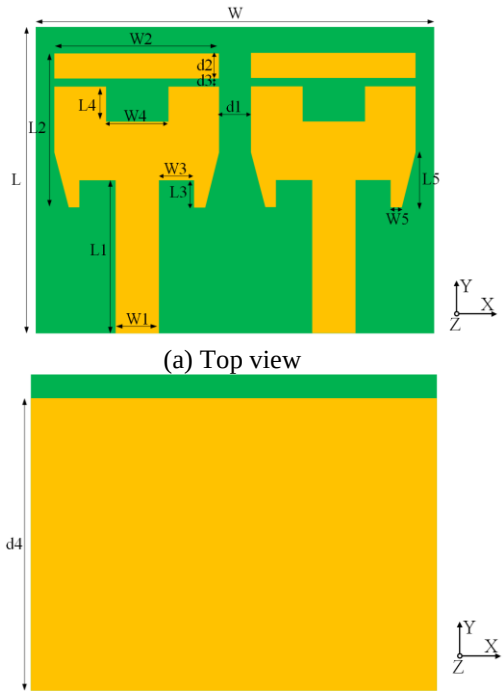

(a) Top view

(b) Bottom view

Fig. 4. Geometry of the proposed MIMO antenna array.

B. Design of the meta-material unit

It is well known that natural materials do not have negative dielectric constant (ε<0) and negative magnetic permeability (μ<0), but the proper design of metamaterials allows it to meet both of above these conditions within the required bandwidth. As we know, the response of a meta-material structure entirely depends on the proper design of its periodic cell. Figure 5 shows the proposed single-layered meta-material cell which consists of two different meta-material structures, a modified double split-rings and a square loop structure. The two structures are printed on the two sides of a FR4 substrate with a thickness (h2) of 0.6 mm. To maintain good isolation over the wide bandwidth, the proposed meta-material cell is further optimized and the finalized parameters of periodic cell are presented in Table 2.

In order to obtain the electromagnetic characteristics of proposed meta-material unit, the meta-material unit is simulated in HFSS Fig. 6 shows the simulation setup; the meta-material unit is placed between two floquet ports and proper boundary conditions including perfectly electric conducting (PEC) and perfectly magnetic conducting (PMC) in the x- and y-direction, respectively. The real and imaginary parts of the S-parameters can be calculated. In [45], the equivalent permittivity can be calculated by the S-parameters, which is presented in formula (1) - (4):

$$z = \pm\sqrt{\frac{(1+S_{11})^2 - S_{21}^2}{(1-S_{11})^2 - S_{21}^2}}, \quad (1)$$

$$e^{jnkd} = \frac{S_{21}}{1 - S_{11}\dfrac{z-1}{z+1}}, \quad (2)$$

$$\varepsilon = \frac{n}{z}, \quad (3)$$

$$\mu = n \cdot z, \quad (4)$$

where k is the wave number of free space, d is the thickness of meta-material unit, n is the refractive index, z is the wave impedance, ε is the equivalent permittivity and μ is the equivalent permeability.

Table 1: The parameters of antenna (Unit: mm)

Parameters	W	W1	W2	W3	W4	W5
Values	30	3	11.7	2.6	4.4	0.75
Parameters	L	L1	L2	L3	L4	L5
Values	22	10.8	11	2	2	2.5
Parameters	h	d1	d2	d3	d4	
Values	1.6	2.3	1.8	0.6	20	

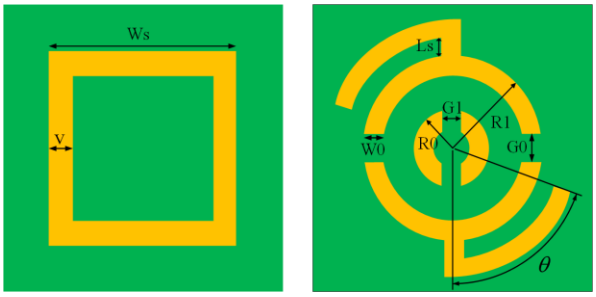

(a) Top view (b) Bottom view

Fig. 5. Configuration of the meta-material cell.

Table 2: The parameters of meta-material cell (Unit: mm)

Parameters	R0	R1	W0	G0	G1
Values	0.8	2	0.4	0.4	0.4
Parameters	Ws	Ls	v	θ	
Values	4	0.4	0.6	40°	

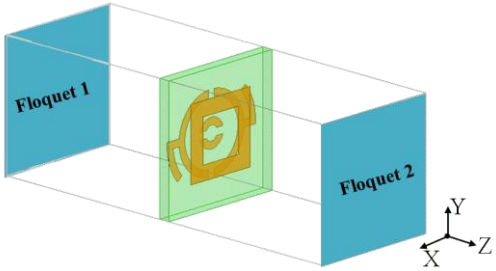

Fig. 6. The electromagnetic model to extract design parameters.

Figure 7 shows the extracted equivalent permittivity and permeability. It is noticed that the unit cell has both a negative permittivity and a negative equivalent permeability in entire X-band.

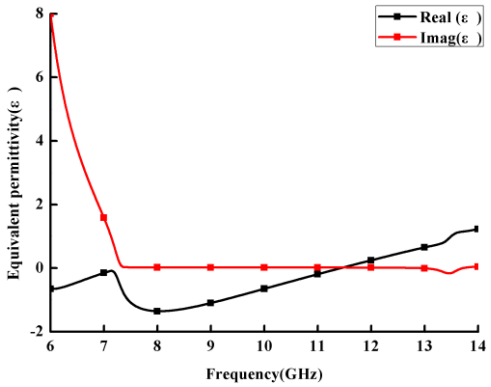

(a) Equivalent permittivity

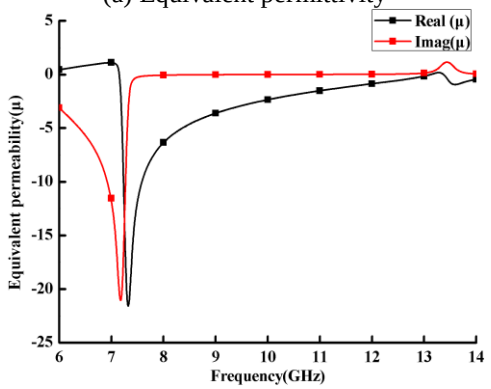

(b) Equivalent permeability

Fig. 7. The equivalent permittivity and permeability of proposed meta-material unit.

C. Analysis of mutual coupling reduction performance

The meta-material superstrate contains 3 × 3 unit cells in the x-axis and y-axis, respectively (Fig. 1). The distance between the centers of each identical periodic cells along the x-axis is 7.5 mm, and the distance along the y-axis is 7 mm. The gap (h1) between the radiating patch and the meta-material layer is 2.1 mm.

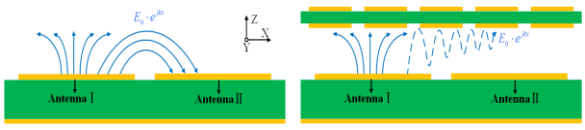

(a) Without superstrate (b) With superstrate

Fig. 8. The radiated field distribution of proposed MIMO antenna array.

Figure 8 illustrates the working principles of the proposed mutual coupling scheme. When the antenna I

is excited, a lateral wave $E_0 e^{jkx}$ propagates along the x-axis can cause an induced current on antenna II, thereby generating mutual coupling between the two antennas. As shown in Fig. 8 (b), a suspended meta-material on the antenna array creates a region of negative magnetic permittivity and permeability:

$$k^2 = \omega^2 \mu\varepsilon\,, \tag{5}$$

$$\vec{S} = \frac{1}{2}\vec{E}\times\vec{H} = \frac{1}{2}\frac{\vec{k}}{\omega\varepsilon}\left|\vec{E}\right|^2 = \frac{1}{2}\frac{\vec{k}}{\omega\mu}\left|\vec{H}\right|^2, \tag{6}$$

$$\vec{k}\cdot\vec{S} = \frac{1}{2}\omega\varepsilon\left|\vec{E}\right|^2 = \frac{1}{2}\omega\mu\left|\vec{H}\right|^2 < 0, \tag{7}$$

where k is the propagation constant of electromagnetic waves, $\vec{S}$ is poynting vector, ε is the permittivity and μ is the permeability.

According to (5) and (7), it can be concluded that the propagation direction of electromagnetic waves is opposite to the energy direction, so the electromagnetic waves propagating along the x-axis direction are gradually attenuated, thereby reducing the coupling of two antennas.

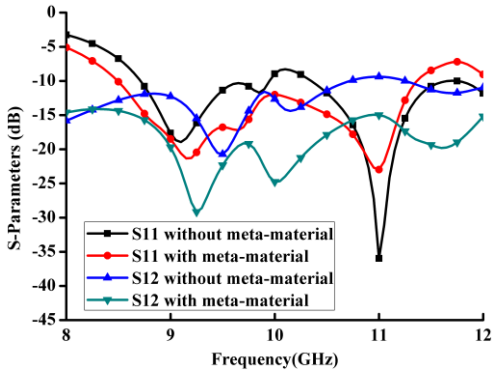

(a) With/without the meta-material superstrate

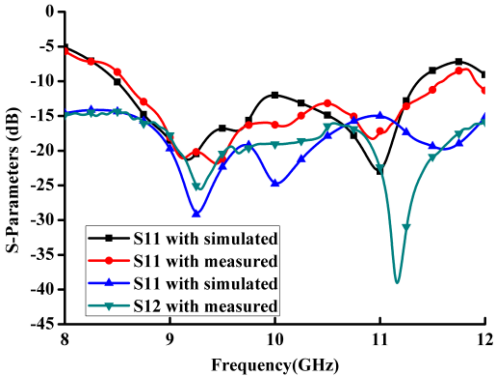

(b) With simulated and measured

Fig. 9. S_{11} and S_{12} of the wideband MIMO directional antenna array.

Figure 9 (a) shows the simulated S-parameters of MIMO directional antenna with and without the meta-material superstrate. It is observed that the meta-material superstrate not only reduces the coupling between the two antennas but also improves the impedance matching of the proposed antenna array. Two resonant frequencies at 9.2 GHz and 11 GHz can be observed. This allows the antenna to cover almost the entire X-band from 8.5 GHz. The mutual coupling is reduced by 6 dB and the resulting leakage between the antennas are better than -15 dB. The measured values of S-parameters are shown in Fig. 9 (b) for a comparison with the simulated values. There is a good agreement between the measurement and the simulation. The small difference between the measurement and the simulation may be attributed to the fabrication tolerances.

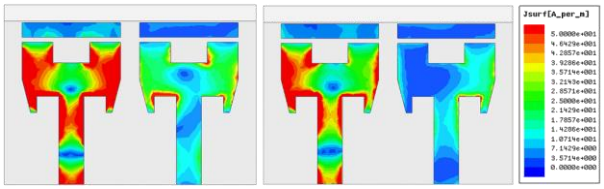

(a) Without/with the decoupling structure at 9 GHz

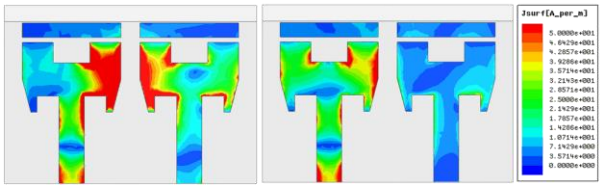

(b) Without/with the decoupling structure at 10 GHz

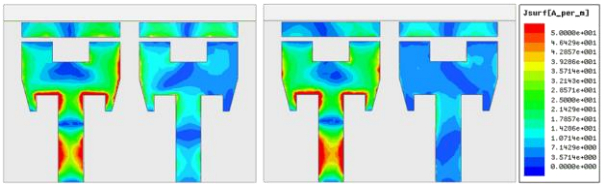

(c) Without/with the decoupling structure at 11 GHz

Fig. 10. Surface current distribution on the proposed MIMO antenna array.

To better understand the working principles of the proposed meta-material superstrate, Fig. 10 plot the current distribution on the antennas with three selected frequencies: f_1 = 9 GHz, f_2 = 10 GHz, f_3 = 11 GHz. In this case, one antenna element is fed, while the other one is terminated. As shown in the left of Figs. 10 (a), (b) and (c), the current distributions on the proposed MIMO antenna without meta-material superstrate is stronger can creates stronger coupling to the adjacent antenna element. After placing the proposed meta-material superstrate above the two antenna elements, it can be observed in the right of Figs. 10 (a), (b) and (c) that the surface current on the right antenna is significantly reduced. Therefore, it is concluded that the proposed meta-material superstrate can isolate the coupling between the two antennas.

III. EXPERIMENTAL VALIDATION

To validate the proposed concept, a prototype antenna array is fabricated and measured. Figure 11 shows a photo the proposed antenna as fabricated according to the aforementioned parameters. The measured results are obtained by the vector network analyzer (VNA) E5063A.

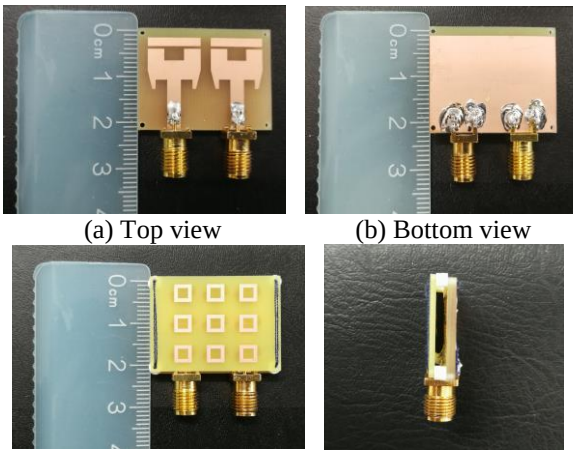

(a) Top view (b) Bottom view

(c) Top view (d) Side view

Fig. 11. Photograph of the fabricated wideband MIMO antenna.

Figure 12 shows the simulated 2D radiation patterns of proposed MIMO directional antenna array with specific frequencies: f_1 = 9 GHz, f_2 = 10 GHz, f_3 = 11 GHz. Because of symmetry, one antenna element is excited, while the other one is terminated with a 50 Ω load. In Fig. 12, although the patterns of antenna fluctuate, the measured data and the simulated data are generally consistent within the allowable errors which are attributed to imperfections in the measurement setup. The proposed antenna array exhibits directional mode of wideband MIMO directional antenna array on the xoz-plane and the yoz-plane and the maximum radiation direction is the z-axis direction. It can be observed that the 3 dB beam-width of xoz-plane are 64º, 62º, 62º and the 3 dB beam-width of yoz-plane are 64º, 64º, 58º, at 9 GHz, 10 GHz, 11 GHz respectively.

In Fig. 13, the gain and efficiency of the proposed wideband MIMO directional antenna are presented with meta-material loading. It can be seen that, from 8.5 GHz to 11.5 GHz, the value of peak gain ranges from 5 dBi to 7.2 dBi and the value of radiation efficiency ranges from 66% to 79%. The maximum gain is 7.2 dBi at 10.1 GHz, and the minimum gain is 5 dBi at 11.5 GHz. Similarly, the maximum efficiency is 79% at 10.35 GHz, and the minimum gain is 66% at 11.5 GHz. Moreover, the variation in the gain values is found to be less than 1.5 dBi and the radiation efficiency is above 70% in the frequency band of 8.5 GHz–11.3GHz. However, the gain and efficiency deteriorate rapidly after 11.3 GHz, and the reason may be that the impedance does not match, resulting in part of the energy to be reflected back on the feedline and not to be effectively radiated from the antenna.

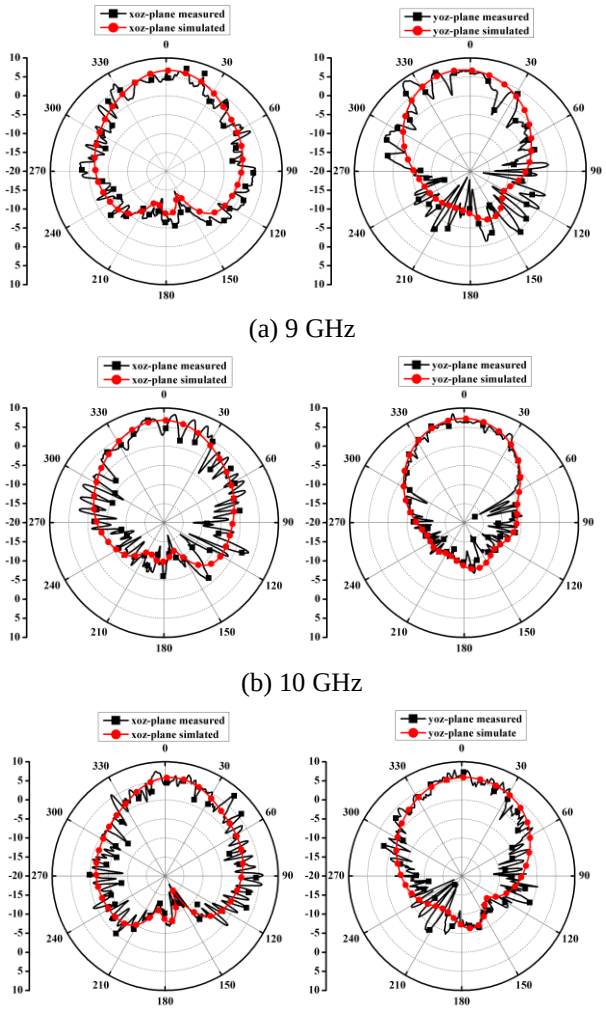

(a) 9 GHz

(b) 10 GHz

(c) 11 GHz

Fig. 12. The simulated and measured radiation patterns.

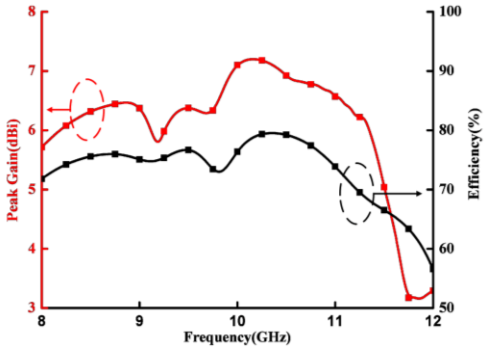

Fig. 13. The Gain and efficiency of the wideband MIMO antenna array.

To further verify the diversity performance of proposed wideband MIMO directional antenna array, the envelope correlation coefficient (ECC), diversity gain (DG) and total effective reflection coefficient (TARC) of the proposed design have been calculated and analyzed.

ECC is defined as a parameter of the level of correlation between antenna elements, and its value takes into account the radiation pattern, the polarization, and the relative phase of fields between them. For the two-element MIMO antenna system, ECC can be given as [46]:

$$\mathrm{ECC}=\frac{\left|S_{11}^{*}S_{12}+S_{21}^{*}S_{22}\right|^{2}}{\left(1-\left|S_{11}\right|^{2}-\left|S_{21}\right|^{2}\right)\left(1-\left|S_{22}\right|^{2}-\left|S_{12}\right|^{2}\right)}. \quad (8)$$

Using the (8), we know that the ECC should be zero in an ideal situation, which is not possible in a real propagation world, even in line of site communication. Theoretically, for good diversity performance, the value of ECC must be less than 0.5 for mobile communication devices. In Fig. 14, the obtained value of ECC is less than 0.01 within the operating frequency band, which indicates that there is very small correlation among the antenna elements.

Another important diversity performance parameter of MIMO communication system is the diversity gain, which is calculated as [47]:

$$\mathrm{DG}=10\times\sqrt{1-\left|\mathrm{ECC}\right|^{2}}. \quad (9)$$

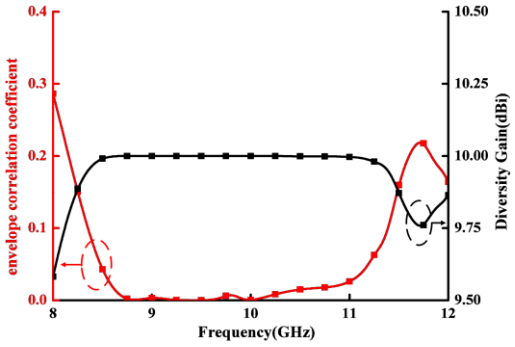

Fig. 14. The ECC and diversity Gain of proposed wideband MIMO directional antenna array.

Therefore, it can be seen from the (9) that the lower ECC, the higher diversity gain and vice versa. As shown in Fig. 14, the diversity gain is approximately 10 dBi from 8.5 GHz to 11.5 GHz.

Similarly, the TARC can be more accurately defined as the actual return loss of the entire MIMO antenna array because it depends on the reflection coefficients, transmission coefficients and the different excitation phase angles. For the two-element MIMO antenna system, the formula for TARC is as follows [48]:

$$\mathrm{TARC}=\frac{\sqrt{\left|\left(S_{11}+S_{12}e^{j\theta}\right)\right|^{2}+\left|\left(S_{21}+S_{22}e^{j\theta}\right)\right|^{2}}}{\sqrt{2}}. \quad (10)$$

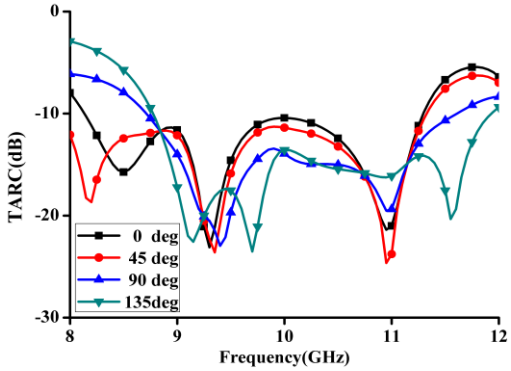

Fig. 15. The TARC of wideband MIMO directional antenna array.

Figure 15 shows the TARC of wideband MIMO directional antenna with four different phase angles: 0^{o}, 45^{o}, 90^{o}, 135^{o}. As can be seen from this figure, the TARC is below -10 dB from 8.5 GHz to 11.5 GHz at any angle, which can explain that the excitation phase angle and the mutual coupling has less influence on the bandwidth of proposed wideband MIMO directional antenna array.

Table 3: Compared to other antennas

Ref.	The Distance between the Two Patches (mm)	Bandwidth (GHz)	Isolation (dB)	The Gap between the Two Layers (mm)
[49]	2.8 (0.034 λ_0)	Narrow band (3.7 and 4.1)	< -26	18 (0.219 λ_0)
[50]	5 (0.095 λ_0)	7.6% (5.6-6.05)	< -24	9 (0.171 λ_0)
[51]	1 (0.019 λ_0)	13.3% (5.6-6.4)	< -15	4.8 (0.086 λ_0)
[52]	18 (0.15 λ_0)	15.6% (2.3-2.69)	< -25	15 (0.219 λ_0)
[53]	4.5 (0.052 λ_0)	11.4% (3.3-3.7)	< -25	15 (0.125 λ_0)
This work	2.3 (0.076 λ_0)	30% (8.5-11.5)	< -15	2.1 (0.070 λ_0)

Finally, the performance of the proposed MIMO antenna array is compared with the other MIMO antenna array using the same techniques of mutual coupling reduction in Table 3. In [49], although this technique can make the coupling further reduced, the bandwidth is narrow. Furthermore, compare to [50-53], the proposed MIMO antenna array has a significantly higher bandwidth than before. In addition, adding dielectric plate above the antenna will inevitably

increase the overall profile thickness. In order to further reduce the thickness, the gap between the two dielectric plates is only 2.1 mm in this design. In summary, the proposed antenna has few advantages, such as compact size, wideband, high isolation and low profile. Additionally, the MIMO antenna can be minimized like [54-57] and designed to be circular polarization antenna [58] or array based on signal processing algorithms [59-65].

IV. CONCLUSION

In this paper, a novel single-layered meta-material superstrate is applied for suppressing mutual coupling of wideband MIMO directional antenna array, where the two antenna elements are in extremely close vicinity. The proposed antenna is designed, optimized, simulated to enhance the performance of antenna. In the entire operating band spanning from 8.5 GHz to 11.5 GHz, the mutual coupling is reduced to be -15 dB. Besides, it can be seen from the radiation pattern that the antenna has good directivity. Meanwhile, the value of peak gain ranges from 5 dBi to 7.2 dBi and the value of radiation efficiency ranges from 66% to 79%, Finally, by analyzing some parameters such as ECC, DG, TARC, it can be concluded that the proposed antenna has good diversity performance. Therefore, the proposed MIMO antenna array using single-layered meta-material decoupling structure would be an attractive candidate for wideband miniaturized wireless communication systems in the future.

ACKNOWLEDGMENT

This work was supported in the Fundamental Research Funds for the Central Universities (3072020CFT0802) and the Key Research and Development Program of Heilongjiang (GX17A016) and Open Project of State Key Laboratory of Millimeter Waves (K202017).

REFERENCES

[1] C. Mao, S. Gao, Y. Wang, Q. Chu, and X. Yang, "Dual-band circularly polarized shared-aperture array for C-/X-band satellite communications," *IEEE Transactions on Antennas and Propagation*, vol. 65, no. 10, pp. 5171-5178, 2017.

[2] J. Kumar, B. Basu, and F. A. Talukdar, "X-band antenna printed on a multilayered substrate," *IET Microwave Antennas & Propagation*, vol. 11, no. 11, pp. 1504-1509, 2017.

[3] B. Mishra, "An ultra compact triple band antenna for X/Ku/K band applications," *Microwave and Optical Technology Letters*, vol. 61, no. 7, pp. 1857-1862, 2019.

[4] X. Zhao, J. Geng, R. Jin, Y. Jin, X. Liu, and W. Yin, "Topological design of planar circularly polarized directional antenna with low profile using particle swarm optimization," *International Journal of Antennas and Propagation*, vol. 2017, pp. 1-12, 2017.

[5] T. Kaiser, F. Zheng, and E. Dimitrov, "An overview of ultra-wide-band systems with MIMO," *Proceedings of the IEEE*, vol. 97, no. 2, pp. 285-312, 2009.

[6] L. Nie, X. Lin, Z. Yang, J. Zhang, amd B. Wang, "Structure-shared planar UWB MIMO antenna with high isolation for mobile platform," *IEEE Transactions on Antennas and Propagation*, vol. 67, no. 4, pp. 2735-2738, 2019.

[7] S. Pahadsingh and S. Sahu, "An integrated MIMO filtenna with wide band-narrow band functionality," *AEU - International Journal of Electronics and Communications*, vol. 110, 2019.

[8] H. H. Tran, N. Hussain, and T. T. Le, "Low-profile wideband circularly polarized MIMO antenna with polarization diversity for WLAN applications," *AEU - International Journal of Electronics and Communications*, vol. 108, pp. 172-180, 2019.

[9] Y. Li, W. Li, and W. Yu, "A multi-band/UWB MIMO/diversity antenna with an enhance isolation using radial stub loaded resonator," *Applied Computational Electromagnetics Society Journal*, vol. 28, no. 1, pp. 8-20, 2013.

[10] Y. Kong, Y. Li, and W. Yu, "A minimized MIMO-UWB antenna with high isolation and triple band-notched functions," *Frequenz*, vol. 70, no. 11-12, pp. 463-471, 2016.

[11] A. Iqbal, O. A. Saraereh, A. W. Ahmad, and S. Bashir, "Mutual coupling reduction using F-shaped stubs in UWB-MIMO antenna," *IEEE Access*, vol. 6, pp. 2755-2759, 2018.

[12] X. Chen, S. Zhang, and Q. Li, "A review of mutual coupling in MIMO systems," *IEEE Access*, vol. 6, pp. 24706-24719, 2018.

[13] I. Nadeem and D. Choi, "Study on mutual coupling reduction technique for MIMO antenna," *IEEE Access*, vol. 7, pp. 563-586, 2019.

[14] B. Pan, W. Tang, M. Qi, H. Ma, Z. Tao, and T. Cui, "Reduction of the spatially mutual coupling between dual-polarized patch antennas using coupled metamaterial slabs," *Scientific Reports*, vol. 6, 2016.

[15] K. Yu, Y. Li, and X. Liu, "Mutual coupling reduction of a MIMO antenna array using 3-D novel meta-material structures," *Applied Computational Electromagnetics Society Journal*, vol. 33, no. 7, pp. 758-763, 2018.

[16] Y. Wang and Z. Du, "A wideband printed dual-antenna with three neutralization lines for mobile terminals," *IEEE Transactions on Antennas and Propagation*, vol. 62, no. 3, pp. 1495-1500, 2014.

[17] S. Zhang and G. F. Pedersen, "Mutual coupling

reduction for UWB MIMO antennas with a wideband neutralization line," *IEEE Antennas and Wireless Propagation Letters*, vol. 15, pp. 166-169, 2016.

[18] S. Luo, Y. Li, Y. Xia, and L. Zhang, "A low mutual coupling antenna array with gain enhancement using metamaterial loading and neutralization line structure," *Applied Computational Electromagnetics Society Journal*, vol. 34, no. 3, pp. 411-418, 2019.

[19] R. Anitha, V. P. Sarin, P. Mohanan, and K. Vasudevan, "Enhanced isolation with defected ground structure in MIMO antenna," *Electronics Letters*, vol. 50, no. 24, pp. 1784-1786, 2014.

[20] C. Luo, J. Hong, and L. Zhong, "Isolation enhancement of a very compact UWB-MIMO slot antenna with two defected ground structures," *IEEE Antennas and Wireless Propagation Letters*, vol. 14, pp. 1766-1769, 2015.

[21] K. Wei, J. Li, L. Wang, Z. Xing, and R. Xu, "Mutual coupling reduction by novel fractal defected ground structure bandgap filter," *IEEE Transactions on Antennas and Propagation*, vol. 64, no. 10, pp. 4328-4335, 2016.

[22] Z. Li, Z. Du, M. Takahashi, K. Saito, and K. Ito, "Reducing mutual coupling of MIMO antennas with parasitic elements for mobile terminals," *IEEE Transactions on Antennas and Propagation*, vol. 60, no. 2, pp. 473-481, 2012.

[23] L. Zhao and K. Wu, "A decoupling technique for four-element symmetric arrays with reactively loaded dummy elements," *IEEE Transactions on Antennas and Propagation*, vol. 62, no. 8, pp. 4416-4421, 2014.

[24] J. Deng, J. Li, and L. Guo, "Decoupling of a three-port MIMO antenna with different impedances using reactively loaded dummy elements," *IEEE Antennas and Wireless Propagation Letters*, vol. 17, no. 3, pp. 430-433, 2018.

[25] J. Ren, W. Hu, Y. Yin, and R. Fan, "Compact printed MIMO antenna for UWB applications," *IEEE Antennas and Wireless Propagation Letters*, vol. 13, pp. 1517-1520, 2014.

[26] S. Rajkumar, K. T. Selvan, P. H. Rao, "Compact 4 element Sierpinski Knopp fractal UWB MIMO antenna with dual band notch," *Microwave and Optical Technology Letters*, vol. 60, no. 4, pp. 1023-1030, 2018.

[27] H. Singh and S. Tripathi, "Compact UWB MIMO antenna with cross-shaped unconnected ground stub using characteristic mode analysis," *Microwave and Optical Technology Letters*, vol. 61, no. 7, pp. 1874-1881, 2019.

[28] J. Lee, S. Kim, and J. Jang, "Reduction of mutual coupling in planar multiple antenna by using 1-D EBG and SRR structures," *IEEE Transactions on Antennas and Propagation*, vol. 63, no. 9, pp. 4194-4198, 2015.

[29] T. Jiang, T Jiao, and Y. Li, "Array mutual coupling reduction using L-loading E-shaped electromagnetic band gap structures," *International Journal of Antennas and Propagation*, vol. 2016, pp. 1-9, 2016.

[30] T. Jiang, T. Jiao, and Y. Li, "A low mutual coupling MIMO antenna using periodic multi-layered electromagnetic band gap structures," *Applied Computational Electromagnetics Society Journal*, vol. 33, no. 3, 2018.

[31] A. Dadgarpour, B. Zarghooni, B. S. Virdee, T. A. Denidni, and A. A. Kishk, "Mutual coupling reduction in dielectric resonator antennas using metasurface shield for 60-GHz MIMO systems," *IEEE Antennas and Wireless Propagation Letters*, vol. 16, pp. 477-480, 2017.

[32] R. Karimian, A. Kesavan, M. Nedil, and T. A. Denidni, "Low-mutual-coupling 60-GHz MIMO antenna system with frequency selective surface wall," *IEEE Antennas and Wireless Propagation Letters*, vol. 16, pp. 373-376, 2017.

[33] Y. Zhao, Y. Li, W. Shi, and W. Yu, "Mutual coupling reduction between patch antenna and microstrip transmission line by using defected isolation wall," *Applied Computational Electromagnetics Society Journal*, vol. 34, no. 1, pp. 100-106, 2019.

[34] M. Akbari, M. M. Ali, M. Farahani, A. R. Sebak, and T. Denidni, "Spatially mutual coupling reduction between CP-MIMO antennas using FSS superstrate," *Electronics Letters*, vol. 53, no. 8, pp. 516-518, 2017.

[35] G. V. Eleftheriades and N. Engheta, "Metamaterials: Fundamentals and applications in the microwave and optical regimes," *Proceedings of the IEEE*, vol. 99, no. 10, pp. 1618-1621, 2011.

[36] S. Bukhari, J. Vardaxoglou, and W. Whittow, "A metasurfaces review: Definitions and applications," *Applied Sciences-Basel*, vol. 9, no. 13, 2019.

[37] F. Qin, S. Gao, Q. Luo, et al., "A simple low-cost shared-aperture dual-band dual-polarized high-gain antenna for synthetic aperture radars," *IEEE Transactions on Antennas and Propagation*, vol. 64, no. 7, pp. 2914-2922, 2016.

[38] Y. Liu, K. Li, Y. Jia, Y. Hao, S. Gong, and Y. J. Guo, "Wideband RCS reduction of a slot array antenna using polarization conversion metasurfaces," *IEEE Transactions on Antennas and Propagation*, vol. 64, no. 1, pp. 326-331, 2016.

[39] H. Baskey and M. Akhtar, "Design of flexible hybrid nanocomposite structure based on frequency selective surface for wideband radar cross section reduction," *IEEE Transactions on Microwave Theory and Techniques*, vol. 65, no. 6,

pp. 2019-2029, 2017.

[40] F. Samadi, M. Akbari, S. Zarbakhsh, R. Chaharmir, and A. Sebak, "High efficient linear polariser using FSS structure," *IET Microwaves, Antennas & Propagation*, vol. 13, no. 1, pp. 88-91, 2019.

[41] J. Zhang, J. Li, and J. Chen, "Mutual coupling reduction of a circularly polarized four-element antenna array using metamaterial absorber for unmanned vehicles," *IEEE Access*, vol. 7, pp. 57469-57475, 2019.

[42] T. Hassan, M. U. Khan, H. Attia, and M. S. Sharawi, "An FSS based correlation reduction technique for MIMO antennas," *IEEE Transactions on Antennas and Propagation*, vol. 66, no. 9, pp. 4900-4905, 2018.

[43] Y. Ranga, L. Matekovits, K. P. Esselle, and A. R. Weily, "Multioctave frequency selective surface reflector for ultrawideband antennas," *IEEE Antennas and Wireless Propagation Letters*, vol. 10, pp. 219-222, 2011.

[44] Y. Cheng, X. Ding, X. Xu, X. Zhong, and C. Liao, "Design and analysis of a bow-tie slot-coupled wideband metasurface antenna," *IEEE Antennas and Wireless Propagation Letters*, vol. 18, no. 7, pp. 1342-1346, 2019.

[45] X. Chen, T. M. Grzegorczyk, B. Wu, J. Pacheco, and J. Kong, "Robust method to retrieve the constitutive effective parameters of metamaterials," *Physical Review E*, vol. 70, no. 1, 2004.

[46] R. G. Vaughan and J. B. Andersen, "Antenna diversity in mobile communications," *IEEE Transactions on Vehicular Technology*, vol. 36, no. 4, pp. 149-172, 1987.

[47] L. Malviya, R. K. Panigrahi, and M. V. Kartikeyan, "MIMO antennas with diversity and mutual coupling reduction techniques: a review," *International Journal of Microwave and Wireless Technologies*, vol. 9, no. 8, pp. 1763-1780, 2017.

[48] S. H. Chae, S. Oh, and S. Park, "Analysis of mutual coupling, correlations, and TARC in WiBro MIMO array antenna," *IEEE Antennas and Wireless Propagation Letters*, vol. 6, pp. 122-125, 2007.

[49] Z. Niu, H. Zhang, Q. Chen, and T. Zhong, "Isolation enhancement in closely coupled dual-band MIMO patch antennas," *IEEE Antennas and Wireless Propagation Letters*, vol. 18, no. 8, pp. 1686-1690, 2019.

[50] R. Mark, N. Rajak, K. Mandal, and S. Das, "Metamaterial based superstrate towards the isolation and gain enhancement of MIMO antenna for WLAN application," *AEU - International Journal of Electronics and Communications*, vol. 100, pp. 144-152, 2018.

[51] Z. Wang, L. Zhao, Y. Cai, S. Zheng, and Y. Yin, "A meta-surface antenna array decoupling (MAAD) method for mutual coupling reduction in a mimo antenna system," *Scientific Reports*, vol. 8, 2018.

[52] L. Zhao, F. Liu, X. Shen, et al., "A high-pass antenna interference cancellation chip for mutual coupling reduction of antennas in contiguous frequency bands," *IEEE Access*, vol. 6, pp. 38097-38105, 2018.

[53] Y. Li, W. Li, and W. Yu, "A multi-band/UWB MIMO/diversity antenna with an enhanced isolation using radial stub loaded resonator," *Applied Computational Electromagnetics Society Journal*, vol. 28, no. 1, pp. 8-20, 2013.

[54] J. Jiang, Y. Xia, and Y. Li, "High isolated X-band MIMO array using novel wheel-like metamaterial decoupling structure," *Applied Computational Electromagnetics Society Journal*, vol. 34, no. 12, pp. 1829-1836, 2019.

[55] P. Xu, S. Luo, Y. Xia, et al., "A low mutual coupling two-element MIMO antenna with a meta-material matrix loading," *Applied Computational Electromagnetics Society Journal*, vol. 34, no. 12, pp. 1851-1856, 2019.

[56] S. Luo, Y. Li, and Y. Xia, "Mutual coupling reduction of a dual-band antenna array using dual-frequency metamaterial structure," *Applied Computational Electromagnetics Society Journal*, vol. 34, no. 3, pp. 403-410, 2019.

[57] J. Li, X. Zhang, X. Chen, et al., "Dual-band eight-antenna array design for MIMO applications in 5G mobile terminals," *IEEE Access*, vol. 7, pp. 71636-71644, 2019.

[58] K. L. Chuang, X. Yan, Y. Li, et al., "A Jia-shaped artistic patch antenna for dual-band circular polarization," *AEÜ- International Journal of Electronics and Communications*, 10.1016/j.aeue.2020.153207.

[59] Y. Li, Z. Jiang, O. M. Omer-Osman, et al., "Mixed norm constrained sparse APA algorithm for satellite and network echo channel estimation," *IEEE Access*, vol. 6, pp. 65901-65908, 2018.

[60] Y. Li, Y. Wang, and T. Jiang, "Sparse-aware set-membership NLMS algorithms and their application for sparse channel estimation and echo cancelation," *AEU - International Journal of Electronics and Communications*, vol. 70, no. 7, pp. 895-902, 2016.

[61] W. Shi, Y. Li, and B. Chen, "A separable maximum correntropy adaptive algorithm," *IEEE Transactions on Circuits and Systems II: Express Briefs*, 10.1109/TCSII.2020.2977608.

[62] B. Chen, Z. Li, Y. Li, and P. Ren, "Asymmetric correntropy for robust adaptive filtering," *IEEE*

Signal Processing Letters, arXiv preprint arXiv:1911.11855.

[63] Q. Wu, Y. Li, Y. V. Zakharov, et al., "A kernel affine projection-like algorithm in reproducing kernel hilbert space," *IEEE Transactions on Circuits and Systems II: Express Briefs*, 10.1109/TCSII.2019.2947317.

[64] W. Shi, Y. Li, L. Zhao, et al., "Controllable sparse antenna array for adaptive beamforming," *IEEE Access*, vol. 7, pp. 6412-6423, 2019.

[65] X. Zhang, T. Jiang, and Y. Li, "A novel block sparse reconstruction method for DOA estimation with unknown mutual coupling," *IEEE Communications Letters*, vol. 23, no. 10, pp. 1845-1848, 2019.